Journal of Hazardous Materials 363 (2019) 109–118

Contents lists available at ScienceDirect

Journal of Hazardous Materials

journal homepage: www.elsevier.com/locate/jhazmat

Synthesis and characterization of La-doped Zn(O,S) photocatalyst for green chemical detoxification of 4-nitrophenol

Hairus Abdullah[a,b], Noto Susanto Gultom[a], Dong-Hau Kuo[a,*]

[a] Department of Materials Science and Engineering, National Taiwan University of Science and Technology, No.43, Sec. 4, Keelung Road, Taipei 10607, Taiwan
[b] Department of Industrial Engineering, Universitas Prima Indonesia, Medan, Indonesia

GRAPHICAL ABSTRACT

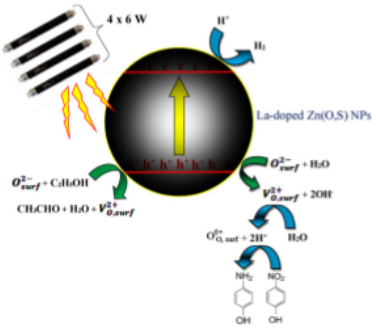

ARTICLE INFO

Keywords:
La-doped Zn(O,S)
4-nitrophenol
4-aminophenol
NaBH4

ABSTRACT

La-doped Zn(O,S) nanoparticles (NPs) with different contents of lanthanum have been synthesized with a simple sol-gel method at low temperature (90 °C) for 4-nitrophenol (4-NP) detoxification. The as-prepared catalysts were characterized with X-ray diffraction (XRD), scanning electron microscope (SEM), high resolution transmission electron microscope (HRTEM), photoluminescence (PL) and UV–vis absorbance spectroscopy, X-ray photoelectron spectroscopy (XPS), electrochemical impedance spectroscopy (EIS), and photoresponsivity. In this work, it is considered that the detoxification of 4-NP to 4-aminophenol (4-AP) without $NaBH_4$ by using photocatalytic method is a green chemical conversion. The experimental data showed 30 ppm toxic 4-NP had been totally converted to useful 4-aminophenol (4-AP) with lower toxicity in 2 h, which was confirmed with a specific peak shift as indicated with UV–vis absorbance spectra and high performance liquid chromatography (HPLC) measurement. The lower amount of evolved hydrogen from photocatalytic process on La-doped Zn(O,S) NPs in the presence of 4-NP confirmed the produced hydrogen was consumed as a reducing agent during the 4-NP-to-4-AP conversion. The photocatalytic detoxification of 4-NP to 4-AP had been demonstrated and an appropriate mechanism based on the experimental data had been proposed and elucidated in this work.

* Corresponding author.
E-mail address: dhkuo@mail.ntust.edu.tw (D.-H. Kuo).

https://doi.org/10.1016/j.jhazmat.2018.09.030
Received 21 May 2018; Received in revised form 8 September 2018; Accepted 10 September 2018
Available online 22 September 2018
0304-3894/

1. Introduction

The highly stable 4-nitrophenol (4-NP) has been noticed its adverse effects to human body. The man-made 4-NP was produced for industrial manufacturing and processing such as to darken leathers, to produce drugs, fungicides, and dyes [1]. There is no evidence that 4-NP is naturally formed, therefore it is a sole responsibility of human to intermediate the chemical. Many efforts [2–4] had been done to detoxify 4-NP to 4-aminophenol (4-AP) which was useful for some applications such as the manufacture of dyes, photographic developers, and antipyretic drugs [5–7]. However, those works utilized sodium borohydride ($NaBH_4$) as a hydrogen source to reduce the nitro to amine groups. No reducing activities are observed without $NaBH_4$ in solution. The excess utilization of $NaBH_4$ which was commonly used to accelerate the reduction reaction could reversely affect our environment due to its corrosive and irritative properties as reported in the material safety data sheet (MSDS). Therefore to find new environmentally friendly and green chemical methods to safely convert toxic 4-NP to less toxic 4-AP in aqueous solution are considerably required. To compare the toxicity of 4-NP and 4-AP as well as other well-known hazardous chemicals, a table with the lethal dose (LD_{50}) which was based on acute oral toxicity experiments for rats was provided in Table 1. LD_{50} value of a substance was the dose required to terminate half the members of a tested population after a specific duration. LD_{50} values were often used as a general indicator of acute toxicity of the substance. A lower LD_{50} value is the indicative of higher toxicity. The LD_{50} values in Table 1 were based on the material safety data sheets (MSDS) and some data from previous works [8,9].

To generate H^+ ions from water by utilizing photocatalyst materials, some requirements such as the valence band of photocatalyst should be positively higher than the water oxidation potential. As the generated H^+ ions were adsorbed on catalyst surfaces, they could be used as a reducing agent for a certain synthesis reaction during the photocatalytic reaction [10]. Otherwise, the generated H^+ ions will be reduced by electron on conduction band to form hydrogen, if the conduction band of photocatalyst is negatively higher than hydrogen reduction potential [11]. Based on the mechanism, it is possible to reduce toxic chemical by utilizing the generated H^+ to form less toxic one. As H^+ ions are either consumed for the reduction reaction or reduced to hydrogen, the reaction solution is safe for the environment and human health. Therefore, hydrogen evolved photocatalysis is identified as one of the promising methods for chemical hydrogenation conversion.

The 4-NP reduction mechanism had been well studied by many previous works [2,4,5,12,13] in the presence of $NaBH_4$ with the availability of H^+ ions on catalyst surfaces as the most critical step in their mechanisms. It is possible to replace the utilization of $NaBH_4$ with hydrogen evolved photocatalysis (HEP) for the hydrogen ion source.

Table 1
Toxicity of various kinds of well-known chemicals with their LD_{50} values.

No.	Chemicals	LD_{50}
1	4-nitrophenol (4-NP)	202 mg/Kg
2	4-aminophenol (4-AP)	375 mg/Kg
3	Paracetamol (acetaminophen)	338 mg/Kg
4	Aspirin	200 mg/Kg
5	Aspartame	10,000 mg/Kg
6	Methyl orange	60 mg/Kg
7	Methylene blue	1,180 mg/Kg
8	Congo red	15,2 mg/Kg
9	Rhodamine B	887 mg/Kg
10	Caffeine	192 mg/Kg
11	Dichlorodiphenyltrichloroethane (DDT)	135 mg/Kg
12	Benzaldehyde	1,300 mg/Kg
13	Benzyl alcohol	1,230 mg/Kg
14	Chloroform	695 mg/Kg
15	Hexavalent chromium	50–150 mg/Kg

The consideration to use HEP is water will be oxidized to form H^+ on catalyst surfaces during the photo-reaction and available for 4-NP reduction. However the lifetime for adsorbed H^+ ions on catalyst surfaces should be long enough before they are reduced to form H_2 gas, otherwise, 4-NP may not be converted to 4-AP. Therefore, a great HEP might be not good for 4-NP reduction if the adsorbed H^+ lifetime was not sufficient for the reduction reaction.

In our previous works, noble metal free Zn(O,S) solid solution was successfully synthesized and utilized for hydrogen production in ethanol solution [11], however, Zn(O,S) was not effective for 4-NP reduction. To enhance the hydrogen evolution reaction and the capability for 4-NP reduction, Zn(O,S) was coupled with Ga_2O_3 to form a nanocomposite. It was found the nanocomposite was effectively used to convert 4-NP to 4-AP in ethanol solution without $NaBH_4$ as a hydrogen source [10]. To the best of our knowledge in this field, only a little work attempted to reduce 4-NP to 4-AP without $NaBH_4$ as a reduction agent. To extend the application of Zn(O,S) based material for 4-NP reduction or another chemical synthesis, several works with metal (M) doping to form (Zn,M)(O,S) solid solution were still in progress.

In this work, it was found Zn(O,S) with rare-earth lanthanum metal doping had a great capability to detoxify 4-NP to form less toxic 4-AP in 10% ethanol solution without $NaBH_4$. La-doped Zn(O,S) was prepared with different La contents to find out an optimum composition for the reduction reaction. The incorporation of La to Zn(O,S) lattice enhanced the adsorbed hydrogen ions on catalyst surfaces and promoted 4-NP reduction. As a result, 30 ppm 4-NP solution can be totally reduced with the presence of La-doped Zn(O,S) in 2 h under low-intensity blacklight UV lamp illumination (0.088 mW/cm^2; $\lambda = 352$ nm). The detail characterization of La-doped Zn(O,S) nanoparticles (NPs) and the mechanism to detoxify 4-NP in ethanol solution were presented and elucidated in this work.

2. Experimental procedure

2.1. Materials

All the chemicals used in this work were commercially available and utilized without further purification treatments.

2.2. Synthesis of La-doped Zn(O,S) NPs

La-doped Zn(O,S) NPs were prepared based on the previous work [11] with the additional $La(NO)_3{\cdot}6H_2O$ precursor. In our typical preparation, 20 mmol zinc acetate dihydrate and 2 mmol $La(NO)_3{\cdot}6\ H_2O$ were first dissolved in 500 mL distilled (DI) water. After all the precursors were well dissolved, 10 mmol thioacetamide (TAA) as sulfur source was added into the reaction solution. During the preparation process, the solution temperature was kept at 90 °C for 4 h. White precipitation was formed during the process and collected with centrifugation. The obtained powder was washed with ethanol for three times and dried at 80 °C in vacuum condition. The obtained powder was named as 10% La-doped Zn(O,S). The other 2.5%, 5%, and 20% La-doped Zn(O,S) NPs were prepared with the same procedure using appropriate amounts of La precursor.

2.3. Characterization

Phase identification of La-doped Zn(O,S) powder was recorded with Bruker D2-phaser diffractometer using Cu Kα radiation with a wavelength of 1.5418 Å. Morphology and microstructure of La-doped Zn(O,S) NPs were examined with field emission scanning electron microscopy (FE-SEM, JSM 6500 F, JEOL, Tokyo, Japan) and high-resolution transmission electron microscope (HRTEM, Tecnai F20 G2, Philips, Netherlands). Diffuse reflectance spectra (DRS) and photoluminescence (PL) of La-doped Zn(O,S) powder were recorded using a Jasco V-670 UV – visible – near IR spectrophotometer. Photo-responses of La-

doped Zn(O,S) NPs were measured in dark chamber with the light source varied from 300 nm to 1000 nm and Keithley-2400 as a power supply. The chamber background response was calibrated with standard Si material which was changeable with samples for measurement. Electrochemical impedance spectroscopy (EIS) measurements of La-doped Zn(O,S) powders were done by using VMP300-based technology, SP-300 Bio-Logic Science Instrument. Glassy carbon electrode (GCE), Ag/AgCl/KCl electrode, and platinum plate were respectively used as the working, reference, and counter electrodes in the measurements. X-ray photoelectron spectroscopy (XPS) measurements of La-doped Zn(O,S) were done on a VG ESCA Scientific Theta Probe spectrometer system with Al Kα (1486.6 eV) source and 15–400 mm X-ray spot size by using ion gun operated at 3 kV and 1 mA. The absorbance peaks of reaction solution before and after photocatalytic reactions were observed with Jasco V-670 UV – visible – near IR spectrophotometer and Hitachi Elite LaChrom high performance liquid chromatography (HPLC). Finally, to confirm the evolved hydrogen was consumed during the 4-NP reduction, the amounts of evolved hydrogen from solution with and without 4-NP in the presence of La-doped Zn(O,S) were determined with gas chromatography (GC-1000). The GC-1000 was equipped with thermal conductivity detector (TCD) and 99.99% Ar as carrier gas. During the measurement, molecular sieve (MS-5 A 60/80; 3.5 m x 1/8″) column was used to identify the evolved hydrogen from reactor.

2.4. Photocatalytic experiment to detoxify 4-NP to 4-AP

In this experiment, 30 ppm 4-NP (450 mL) was used to evaluate the reduction capability of La-doped Zn(O,S) NPs under low power blacklight UV tube lamp illumination (0.088 mW·cm^{-2} based on the photometer measurement). The UV light source consisted of 4 × 6 W blacklight UV tube lamps which were inserted in the middle of reactor. The lamps which usually used for banknote detector had low intensity, therefore this experiment did not need water cooling during the photocatalytic experiments. To detoxify the 30 ppm 4-NP solution, 225 mg catalyst powder was well dispersed in 450 mL 4-NP solution. Ar gas with the purity of 99.99% was continuously flowed through the reactor to eliminate all the atmospheric gases in reactor during photocatalytic reduction reaction. Aliquots were taken from the reaction solution in the time interval of 15 min during the experiment and were examined with UV–vis spectroscopy. The existences of 4-NP and 4-AP were observed with the UV absorbance peaks at 316.4 and 298.7 nm, respectively. To ensure the conversion of 4-NP to 4-AP, the aliquots for 0 h, 1 h, and 2 h photocatalytic reactions were also investigated with high performance liquid chromatography (HPLC) measurement. The schematic experimental set up was provided in Fig. S3 in supplementary data.

2.5. Photocatalytic hydrogen evolution experiment

The experiment was carried out in the same reactor which used for 4-NP reduction under 4 × 6 W blacklight UV tube lamps illumination. This experiment was done to show the produced hydrogen on catalyst surfaces was used for 4-NP detoxification. For this purpose, the experiment was conducted by dispersing 225 mg catalyst powder in 450 mL ethanol solution (10% v/v) with and without 30 ppm 4-NP. Prior to starting the experiment, the reactor was purged with 99.99% Ar to remove all the atmospheric gases. The experiment was for 3 h and the produced gas from the reactor was hourly sampled by flowing Ar gas through the reactor to GC machine. During the GC measurement, the produced gas in reactor was flowed at 100 cc/min to GC system and the amount of hydrogen gas was determined by the peak area with the retention time at 0.6 min.

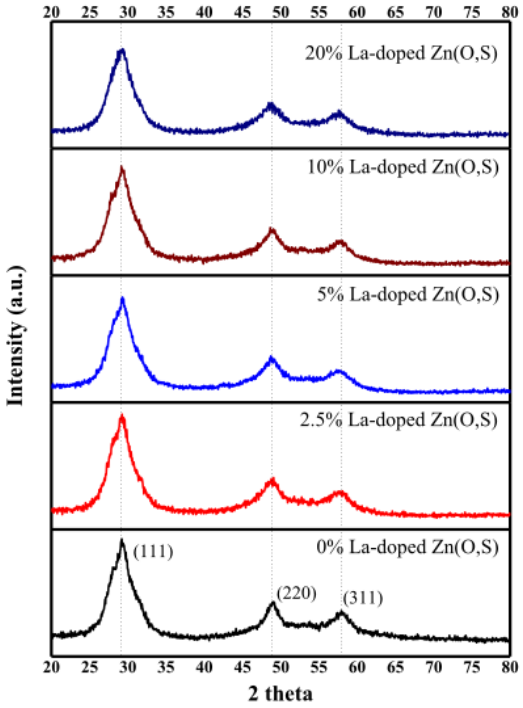

Fig. 1. XRD patterns of La-doped Zn(O,S) powders with different La contents.

3. Results and discussion

3.1. X-ray powder diffraction pattern

Firstly, to clearly indicate the solid solution formation of Zn(O,S), the XRD pattern of Zn(O,S) was compared to cubic ZnO (PDF#65-2880) and ZnS (PDF#05-0566) in Fig. S1 (supplementary data). Fig. S1 showed Zn(O,S) peak pattern about La doping for (111), (220), and (311) planes was shifted and located between those of ZnO and ZnS patterns. The peak shift is attributed to the formation of Zn(O,S) solid solution, in which the O^{2-} anions (140 pm) [14] occupied the S^{2-} anions (184 pm) [14] in ZnS lead to smaller lattice parameter. A comprehensive discussion about Zn(O,S) NPs had been well discussed in our previous work [11].

The phase formations of different La-doped Zn(O,S) NPs were examined with X-ray diffraction (XRD) patterns. Fig. 1 showed the sphalerite or zinc blende patterns of La-doped Zn(O,S) with different La contents. Based on the Scherrer equation for the (111) peak, all of the La-doped Zn(O,S) powders had a calculated crystalline size about 2.5 nm. The observed patterns in Fig. 1 did not show any differences for different La contents, indicating the formation of La-doped Zn(O,S) solid solution. Although the ion radii of La is larger than that of Zn, the peak shift in XRD pattern was not obviously occurred due to the small amount of La that could be incorporated into Zn(O,S) lattice. The actual amount of La in Zn(O,S) system was examined based on the energy dispersive X-ray spectroscopy (EDS) analysis as indicated in Table 2.

3.2. High resolution transmission electron microscopy (HRTEM) analysis

The morphology of as-prepared 10% La-doped Zn(O,S) was investigated with HRTEM analysis. Fig. 1 indicated La-doped Zn(O,S) contained of tiny particles (about 2.5 nm as confirmed by Scherrer equation) that naturally aggregated to form a larger particle with the size about 50 nm. The lattice fringe image and selected area electron diffraction (SAED) pattern which were presented in Fig. 2b and c

Table 2
Energy dispersive X-ray spectroscopy (EDS) analysis of different La contents doped in Zn(O,S) NPs.

As-designed percentages	Actual percentages
2.5% La	0.12 %
5% La	0.20 %
10% La	0.40 %
20% La	0.51 %

suggested the multi-quantum well (MQW) formation of La-doped Zn(O,S). The formation of MQW was indicated by different lattice fringe values at (111) which were found in the range between the lattice parameter values of d(111) ZnS = 3.12 Å (PDF#05-0566) and d(111) ZnO = 2.67 Å (PDF#65-2880) as shown in Fig. 2b. Moreover, the broad ring pattern in SAED in Fig. 2c was also consistent to the varying lattice fringe values in Fig. 2b. To show it clearly, the inner and outer depicted ZnS and ZnO ring patterns were provided in Fig. 2c. The broad ring pattern of La-doped Zn(O,S) at (111) was located between the depicted ring patterns, suggesting there were many lattice fringe values which formed between those of ZnS and ZnO to naturally establish the MQW of La-doped Zn(O,S). A complete discussion of MQW formation had been provided in our previous work [11], therefore there was no discussion about it in this present work. All the elements in La-doped Zn(O,S) were confirmed with HRTEM element mapping. High angle annular dark field (HAADF) image with the depicted red rectangle area for element mapping in Fig. 3 indicated the as-prepared 10% La-doped Zn(O,S) NPs contained of Zn, La, O, and S elements. However, the La mapping image was not as dense as others, indicating the amount of La in the nanoparticles was much lower compared to others.

3.3. Optical properties of La-doped Zn(O,S) NPs

The optical properties were examined with diffuse reflectance spectroscopy (DRS) and photoluminescence (PL) measurements. The UV light absorbances of Zn(O,S) at 250–320 nm (UV−B range) was significantly increased after doped with different amounts of La as shown in Fig. 4a. However, UV−B lamp was not utilized in this work due to safety issue. As the light illumination wavelength was 352 nm in this work, a dash line was marked at that wavelength position in Fig. 4a and it showed the highest intensity was found at 10% La content. To find out the bandgap values of as-prepared catalysts, a related Tauc plot was delineated for each catalyst to determine its bandgap as shown in Fig. 4b. Tauc plot was determined by the formula of $\alpha h\nu = A(h\nu - Eg)^m$ for $Eg > h\nu$ and $\alpha h\nu = 0$ for $Eg < h\nu$. In where α is the material optical absorbance, $h\nu$ is the photon energy, Eg is bandgap energy value, and m = 0.5 and 2 for materials with direct and indirect allowed transition bandgap, respectively.[15] The bandgap values of La-doped Zn(O,S) for all compositions were increased about 0.1 eV as compared with that of Zn(O,S). To characterize the recombination rate for each catalyst, PL measurement was carried out and the result was provided in Fig. 5. Photoluminescence emission intensity was related to the recombination rate of photo carriers after excitation process. The higher the emission intensity is, the higher recombination rate of photo carriers will be occurred after illumination. In this case, 10% La-doped Zn(O,S) exhibited the lowest emission intensity which was important for a photocatalytic process, since lower emission intensity indicated longer lifetime of photo carriers to provide reduction reaction for 4-NP. Based on the DRS and PL measurement, 10% La-doped Zn(O,S) catalyst was selected to detoxify 4-NP in this work.

3.4. X-ray photoelectron spectroscopy (XPS) analysis

The chemical state of 10% La-doped Zn(O,S) was examined with XPS analysis to ensure the appropriate value of binding energy for each

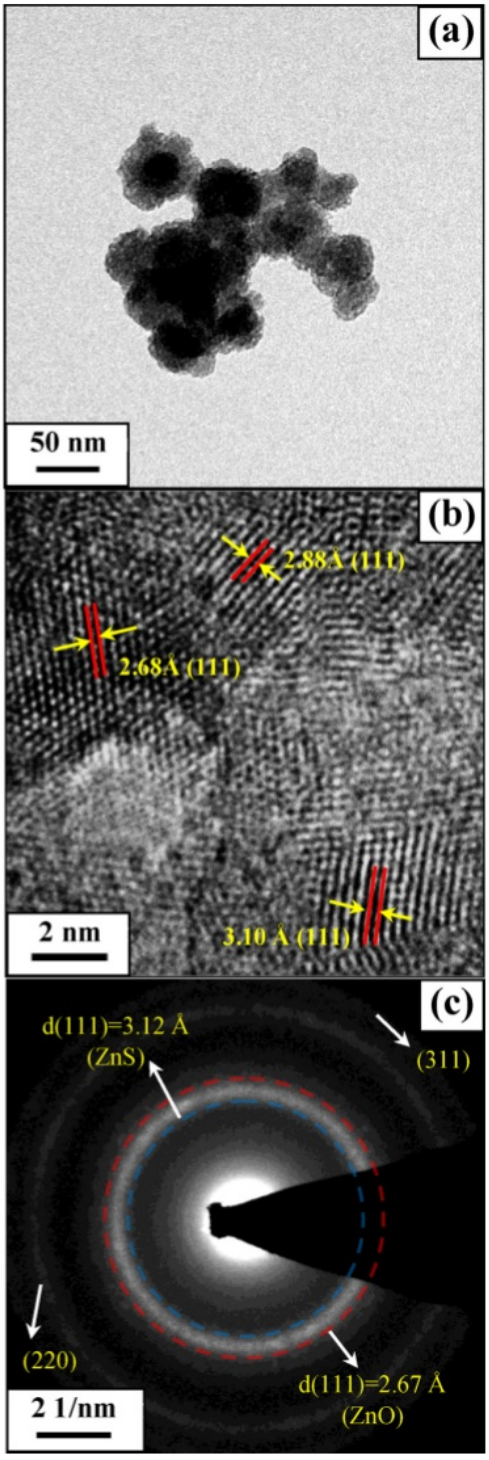

Fig. 2. HRTEM images of (a) La-doped Zn(O,S) at low magnification, (b) lattice fringes of La-doped Zn(O,S), and (c) selected area electron diffraction (SAED) of La-doped Zn(O,S) with the depicted ring patterns for standard ZnS and ZnO at (111) plane.

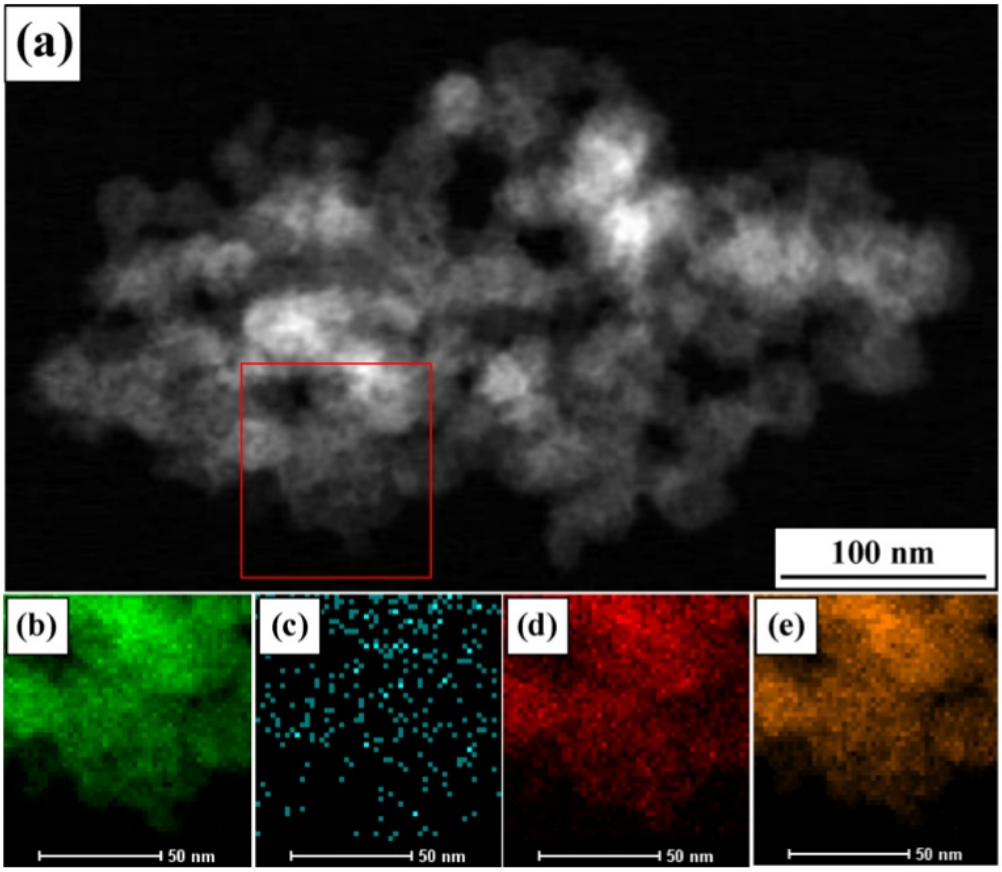

Fig. 3. (a) HAADF image and element mapping of (b) Zn, (c) La, (d) O, and (e) S in La-doped Zn(O,S) nanoparticles as indicated with red rectangle on figure (a) (For interpretation of the references to colour in this figure legend, the reader is referred to the web version of this article).

element in catalyst. The XPS high resolution scans for Zn, O, S, and La elements were respectively shown in Fig. 6a–d. The binding energy values of Zn ($2p_{3/2}$) and Zn ($2p_{1/2}$) in ZnOS-0.5 were noticed at 1021.7 and 1044.9 eV, respectively, which were consistent with our previous work. [10,11] The oxygen binding energy values were found at 530.6 eV, 531.6 eV, and 532.2 eV which were related to oxygen in lattice (O_L), oxygen vacancy site (O_V), and adsorbed oxygen (O_{ads}) as hydroxides attached on catalyst surfaces, respectively. All the binding energy values of oxygen were agreed with our previous work [11]. Based on the peak areas, the amounts of oxygen in lattice (O_L), oxygen vacancy site (O_V), and adsorbed oxygen (O_{ads}) were 70%, 14%, and 16%, respectively. The presences of S ($2p_{3/2}$) and S ($2p_{1/2}$) peaks were respectively confirmed with the binding energy values at 161.6 eV and 163.79 eV, which were consistent to previous work [16]. Finally, the La ($3d_{5/2}$) and La ($3d_{3/2}$) peaks were found at 834.19 eV and 850.87 eV, respectively [17]. However, the peak intensities were much lower compared to other peaks due to the small amount of La doped into Zn(O,S) as confirmed with the EDS and element mapping analysis.

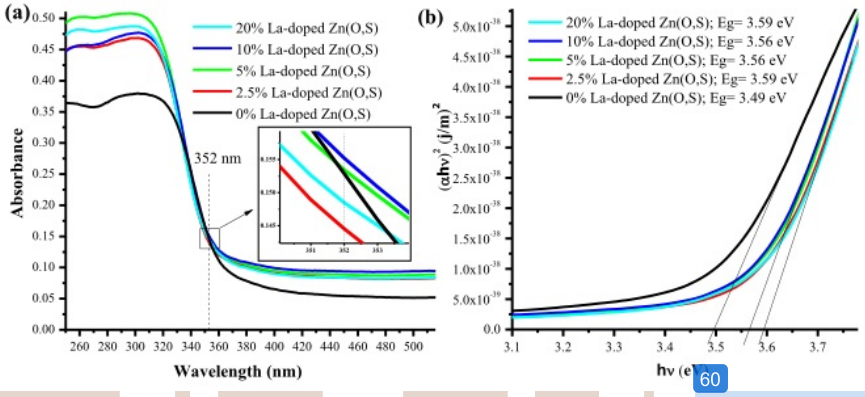

Fig. 4. (a) Diffuse reflectance spectra (DRS) of La-doped Zn(O,S) powders with different La contents and (b) the Tauc plot for bandgap value determination.

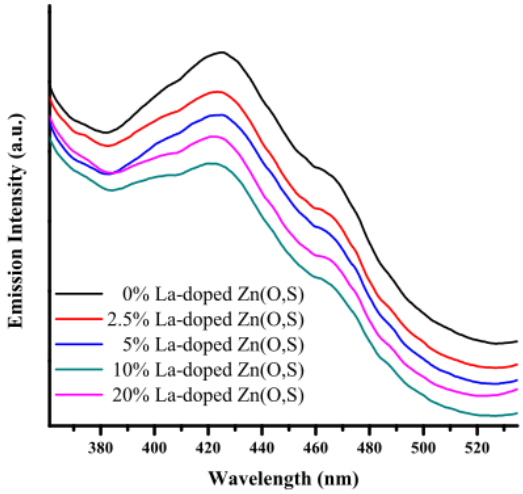

Fig. 5. Photoluminescence (PL) spectra of La-doped Zn(O,S) with different La contents.

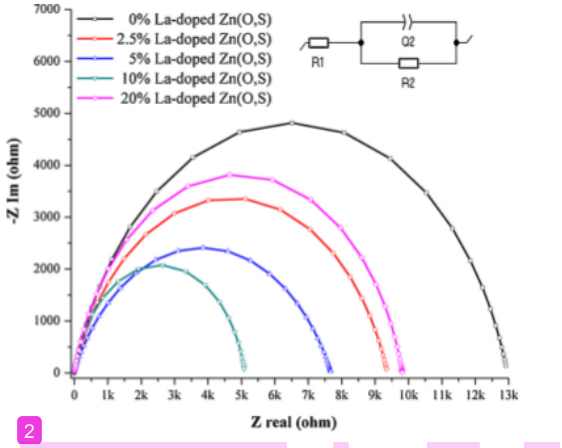

Fig. 7. Electrochemical impedance spectra (EIS) of La-doped Zn(O,S) NPs with different La contents and the Randles equivalent circuit for curve fitting as shown in the inset.

3.5. Electrochemical impedance spectroscopy (EIS) analysis

EIS analysis was used to understand the electrochemical property of La-doped Zn(O,S) NP powders for different La contents. EIS measurement is the powerful tool to determine the electrical resistance between the catalyst coated glassy carbon electrode and electrolyte. The capacitive double layer between them will be formed at the interfaces and gives a specific semicircle spectrum in Nyquist plot. The smaller semicircle indicated the lower electron transfer resistance at the interface between catalyst and electrolyte. The measurement was conducted in 0.1 M KCl electrolyte solution with the frequency range from 200 KHz

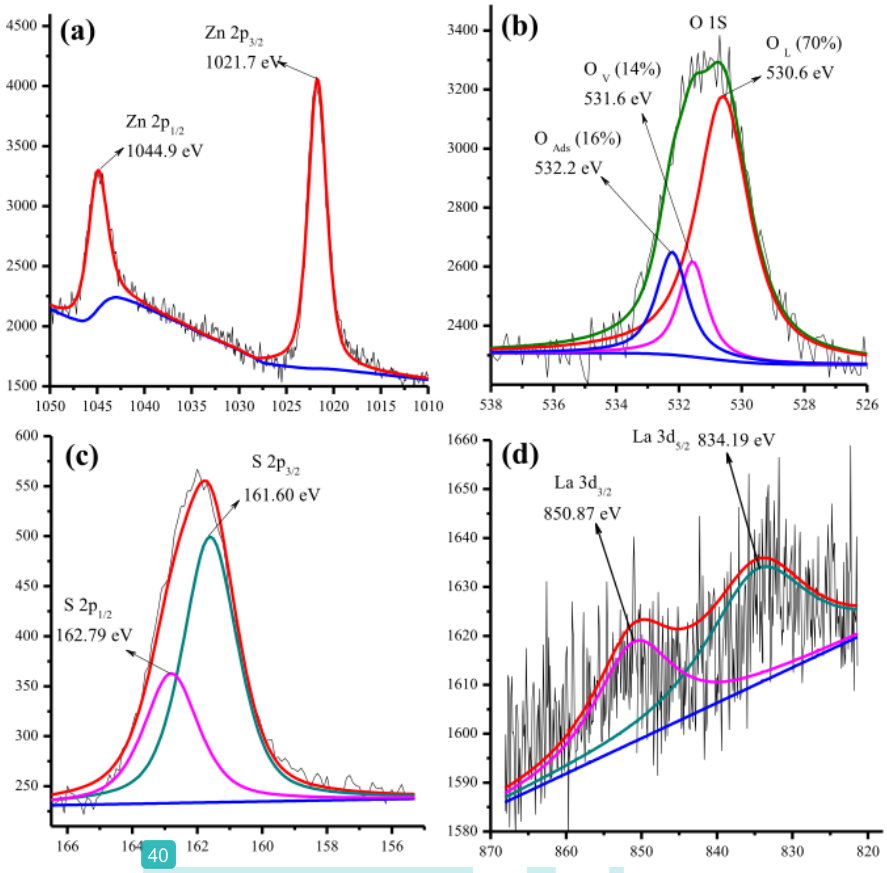

Fig. 6. High resolution XPS spectra of Zn 2p, O 1S, S 2p, and La 3d in La-doped Zn(O,S) NPs.

to 100 mHz, window potential and signal amplitude were set from -5 – 5 V and 10 mA, respectively. The deposition of catalyst powder on GCE was done by dropping catalyst dispersed nafion solution on GCE surface which was dried at 80 °C in air. The catalyst dispersed solution was prepared with 5 mg photocatalyst powder that well dispersed in 1 mL Nafion solution (DI water : isopropanol = 3 : 1). Fig. 7 showed the EIS spectra for La-doped Zn(O,S) with different amounts of La and Randles fitting which was done to estimate the electron transfer resistance for each catalyst during the electrochemical measurement. The symbols of R_1, R_2, and Q_2 were related to the electrolyte resistance, electron transfer resistance, and double layer capacitance, respectively. Based on the Randles fitting, the calculated electron transfer resistance values of 0%, 2.5%, 5%, 10%, 20% La-doped Zn(O,S) modified GCE were 12.96 KΩ, 9.35 KΩ, 7.71 KΩ, 5.10 KΩ and 9.83 KΩ, respectively. The lowest electron transfer resistance was found in 10% La-doped Zn(O,S), indicating the most efficient electron transfer in the interfaces between electrode and electrolyte during the electrochemical measurement. Based on the EIS measurement, 10% La-doped Zn(O,S) was possibly a great photocatalyst material for 4-NP detoxification.

3.6. Photo-response analysis

Photo-response property is an important characterization for photo-driven materials such as photocatalyst. To show the as-prepared La-doped Zn(O,S) NPs with great responses to the incoming light irradiation, the different La-doped Zn(O,S) NPs (0%, 2.5%, 5%, 10%, and 20%) were dispersed in Nafion solution (5 mg/mL) and coated on Pt substrate (3 mm^2) which was sputtered on glass. Ag paste was used as the connecting electrodes to increase the electrical current during the photo-response measurement. Prior to starting the measurement, a drop of 0.1 M KCl electrolyte was used to connect the electrodes as shown in the schematic diagram for experimental photo-response in Fig. 8a. To identify the wavelength of light absorbance peak for photo-response measurement, one of the catalyst-coated Pt electrode was illuminated with 300–1000 nm light irradiation and the generated electrical signal was detected. Fig. 8a showed the maximum light absorbance was found at 330 nm which was close to the bandgap values of La-doped Zn(O,S) NPs. The photo current as shown in Fig. 8b was observed as the catalyst-coated electrode was illuminated with 330 nm light. The peaks in the photo current vs time spectra in Fig. 8b represented a light-on condition for 5 s, however the tails of the peaks were quite long to achieve steady-state (light-off) condition which was set for 20 s. The long tails of the peaks indicated the as-prepared La-doped Zn(O,S) catalysts had sufficient lifetime to provide the photo reactions. Based on the photo-response data, the photo-generated currents were 0.003, 0.003, 0.018, 0.035, and 0.0125 μA for 0%, 2.5%, 5%, 10%, and 20% La-doped Zn(O,S) NPs, respectively. The highest photo-generated current was occured for 10% La-doped Zn(O,S) which was consistent with DRS, PL, and EIS data.

3.7. UV–vis absorbance analysis for photocatalytic reaction

After characterization for La-doped Zn(O,S) with different La contents, it was found that 10% La-doped Zn(O,S) exhibited a low recombination rate of photo carrier and a great electron transfer property with lower resistance as confirmed with PL and EIS measurements, respectively. Furthermore, the amount of hydrogen evolution on 10% La-doped Zn(O,S) was found as the highest one compared to other catalysts with different La contents as shown in Fig. S4 (supplementary data) which was also consistent with other properties in PL, EIS, and photo-response measurements. Therefore, the catalyst with 10% La doping was utilized to detoxify 30 ppm 4-NP under 352 nm blacklight UV tube lamp illumination. To understand the 4-NP reduction mechanism, the experiments with different conditions, i.e., (1) 30 ppm 4-NP + 10% ethanol solution, (2) 30 ppm 4-NP + 10% La-doped Zn(O,S) catalyst, and (3) 30 ppm 4-NP + 10% ethanol solution + 10% La-doped Zn(O,S) catalyst were separately prepared in 450 mL solution and tested under UV blacklight illumination to observe the conversion of 4-NP to 4-AP. During the photocatalytic reaction, an aliquot was taken in a certain time interval and its light absorbance was examined with UV–vis spectroscopy. The UV–vis absorbance spectra with different experimental conditions were shown in Fig. 9. The existences of 4-NP and 4-AP in reaction solution were identified based on the absorbance peaks at 316.4 nm and 298.7 nm, respectively, as shown in our previous work. [2,10] The UV–vis absorbance spectra with different experimental conditions suggested that there was no reduction reaction

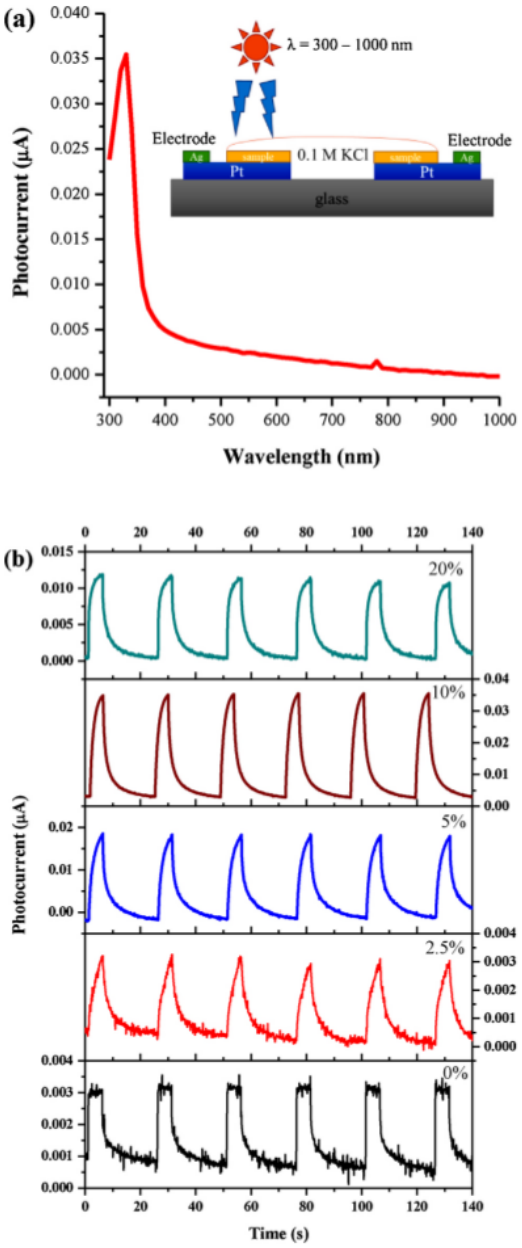

Fig. 8. Photo-responsivity of (a) 10% La-doped Zn(O,S) under light illumination with different wavelength illumination and (b) photo current-time spectra of La-doped Zn(O,S) with different La contents under 330 nm light illumination. The set up experiment was shown in the inset in figure (a).

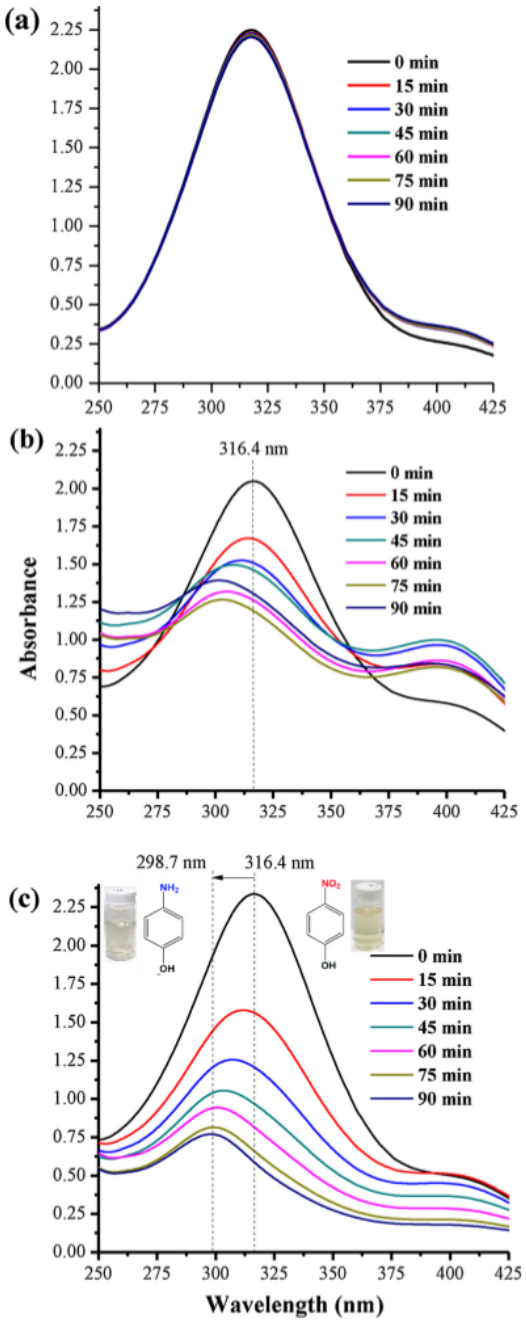

Fig. 9. UV–vis absorbance spectra of (a) 30 ppm 4-NP + 10% ethanol solution, (b) 30 ppm 4-NP + 10% La-doped Zn(O,S) catalyst, and (c) 30 ppm 4-NP + 10% ethanol solution + 10% La-doped Zn(O,S) catalyst with different 24 W UV-light illumination periods.

occurred in the solution containing 30 ppm 4-NP and 10% ethanol without catalyst as shown in Fig. 9a, since the absorbance peak shift was not observable. In the other case, the solution with 30 ppm 4-NP and catalyst without ethanol showed a little peak shift to a lower wavelength near 298.7 nm as shown in Fig. 9b, however the absorbance peak did not respectively shift with reaction time due to the low evolved-hydrogen amount without ethanol as a hole scavenger agent.

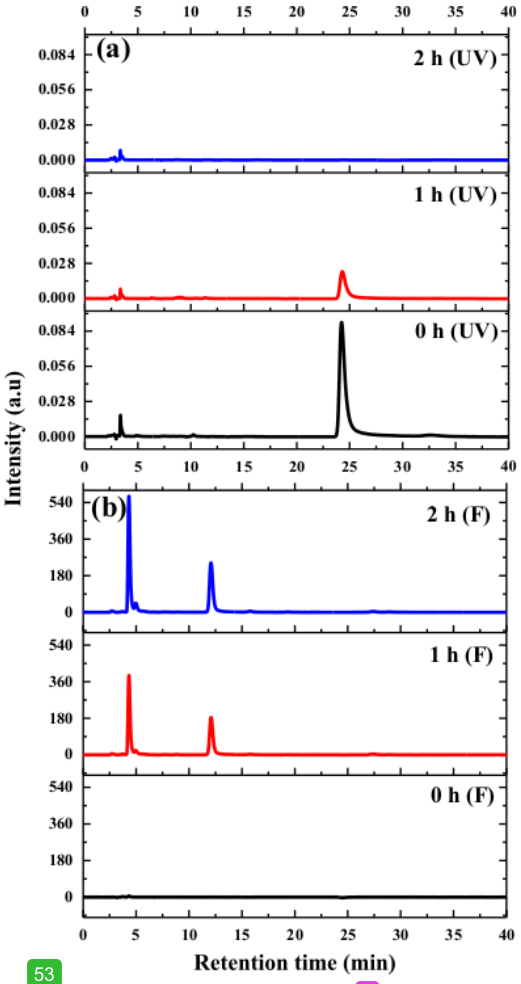

Fig. 10. High performance liquid chromatography (HPLC) spectra of (a) 4-NP and (b) 4-AP solution after photocatalytic reduction in the presence of 10% La-doped Zn(O,S) with different reaction time using UV and fluorescent detectors, respectively.

Based on the peak shift from 316.4 nm to 298.7 nm in Fig. 9c, the detoxification of 4-NP to 4-AP had been obviously occurred in the reaction solution that containing 4-NP, 10% ethanol, and 10% La-doped Zn(O,S) catalyst. The yellowish color of 4-NP solution and clear solution of 4-AP was observed with the absorbance peaks at 316 nm and 298.7 nm, before and after photo reaction, respectively, as shown in the inset in Fig. 9c. The experimental data suggested the utilization of ethanol as a hole scavenger agent was a critical step to evolve hydrogen as a reduction agent on catalyst surface during the 4-NP reduction. To show the important effect of La doping in this work, the pure Zn(O,S) NPs was also tested with the same condition as Fig. 9c and the result was shown in Fig. S2 in supplementary data. Without La-doped into Zn(O,S) lattice, only photodegradation of 4-NP (without peak shift) was observed instead of photo reduction.

3.8. High performance liquid chromatography (HPLC) analysis

To ensure the UV–vis results that 30 ppm 4-NP solution had been reduced to 4-AP with 10% La-doped Zn(O,S) catalyst in the presence of 352 nm UV blacklight lamp, the aliquots for 0, 1, 2 h reactions were carefully examined with HPLC machine. During the HPLC

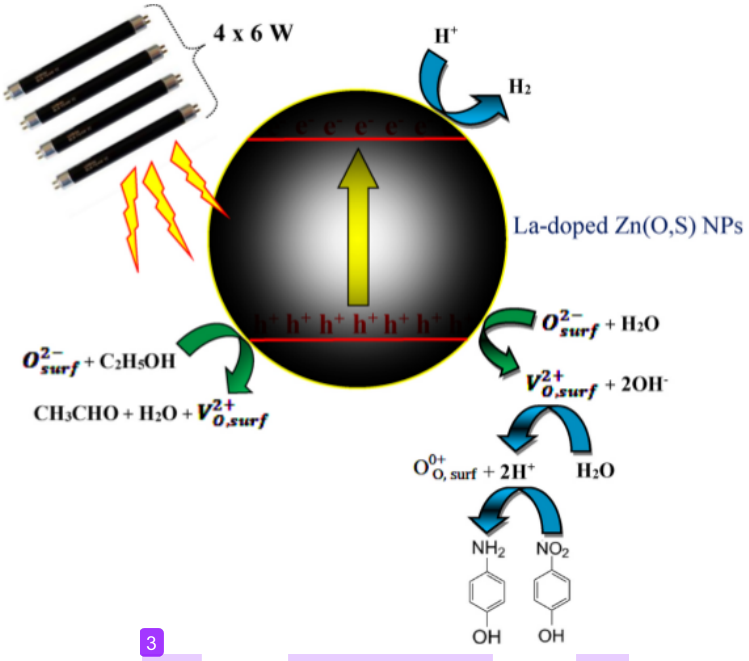

Fig. 11. Photocatalytic detoxification mechanism of 4-NP reduction to 4-AP in the presence of La-doped Zn(O,S) NPs under 4 × 6 W blacklight UV tube lamp illumination.

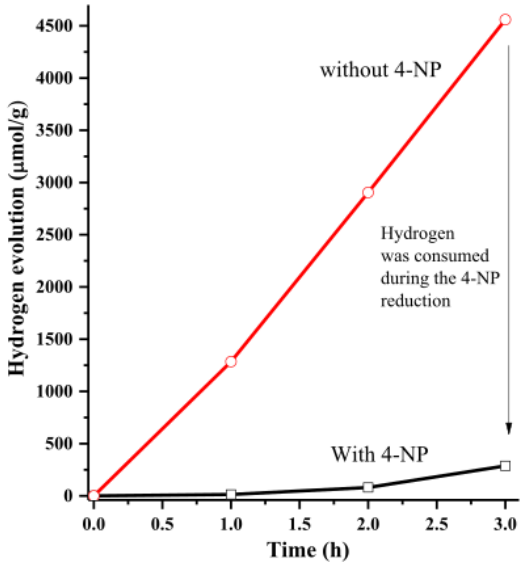

Fig. 12. Hydrogen evolution amount of La-doped Zn(O,S) with and without 4-NP in 10% ethanol solution.

measurement, a reversed phase liquid chromatography C-18 column was used with 20% methanol solution containing 5 mM tetrabutylammonium phosphate (TBAP) as mobile phase to separate 4-NP and 4-AP in the aliqouts. The measurement was operated at room temperature with the flow rate of 1 mL/min and the amount of sample intake was 50 µL for each aliquot. The existences of 4-NP and 4-AP in the aliquots were respectively observed with UV and fluorescent detectors with the retention times about 25 min and 5 min. The observation wavelengths for UV and flourescent detectors were both at 323 nm. The chromatograms with the decreasing peak intensities of 4-NP and the increasing peak intensities of 4-AP after reactions proceeded from 0 to 2 h were shown in Fig. 10a and 10b, respectively. The additional peak at 12.5 min which was attributed to polymerization product of 4-AP was also observed during the monitoring of 4-AP in Fig. 10b. All the peak positions for 4-NP, 4-AP, and the 4-AP polymerization product were confirmed with commercial 4-NP and 4-AP with the same measurement condition. The polymerization product was easily observed from its brown color solution after several days since the 4-AP formation. Based on the chromatograms in Fig. 10, it is confirmed that 4-NP has been totally reduced to form 4-AP in 2 h photo reaction. The amounts of 4-NP and 4-AP and its polimerization products with respect to reaction time were calculated and presented in Fig. S5 based on HPLC measurements.

3.9. Photocatalytic reduction mechanism to detoxify 4-NP

The photocatalytic reduction will be initiated with photoexcitation to form hole and electron in the valence and conduction bands, respectively [2,10,11,15,18]. Based on our previous works [10,11], the photo reaction with Kröger-Vink notation was proposed as follows:

$$La - doped\ Zn(O,S) \xrightarrow{Photon} h^+ + e^- \quad (1)$$

$$H_2O + O^{2-}_{surf} + 2h^+ \rightarrow 2OH^-_{aq.} + V^{2+}_{O,surf} \quad (2)$$

$$C_2H_5OH + O^{2-}_{surf} + 4h^+ \rightarrow CH_3CHO + H_2O + V^{2+}_{O,surf} \quad (3)$$

$$H_2O + V^{2+}_{O,surf} \rightarrow 2H^+ + O^{0+}_{o,surf} \quad (4)$$

$$2H^+ + 2e^- \rightarrow H_2 \quad (5)$$

As shown in the Eqs. ((1)–(5)), the photo-generated hole together with the adsorbed oxygen anion on catalyst surfaces can oxidize water and ethanol. The water and ethanol oxidation as shown in Eqs. (2) and (3) will produce oxygen vacancy sites which are critical to reduce water and to form H^+ ions as shown in Eq. (4). As long as the produced H^+ ions on catalyst surfaces are not reduced by photo-generated electron as shown in Eq. (5), they are readily for 4-NP reduction. The schematic

drawing of the proposed mechanism is shown in Fig. 11. The availability of 4-NP in solution after H^+ formation and the positive charge on catalyst surface will easily attract 4-NP on catalyst surfaces due to electrostatic interactions. [19] At the same time, the existence of the surplus photo-generated electrons on catalyst surfaces induced the uptake of electrons by the adsorbed 4-NP molecules. Furthermore, the availability of H^+ on catalyst surfaces led to the reduction of 4-NP into 4-AP products. The critical role of H^+ ions on catalyst surfaces to reduce 4-NP had been elucidated by many other works. [2,5,13,19,20] However, all of the works used $NaBH_4$ as the source of hydrogen for their reduction reaction. In order to confirm the reaction mechanism, photocatalytic hydrogen evolution experiments were conducted and the results were shown in Fig. 12. The evolved hydrogen amount in the presence of 4-NP in ethanol solution was obviously lower than that without 4-NP, indicating the evolved hydrogen ion was consumed by the photocatalytic reduction reaction during the detoxification of 4-NP reduction. The result in Fig. 12 also confirmed the produced H^+ ions on catalyst surface were an important step to 4-NP reduction as asserted by many other works in this field.

4. Conclusions

La-doped Zn(O,S) photocatalysts with different La contents had been synthesized with solution based method at low temperature and successfully utilized to detoxify 4-NP solution. The as-prepared catalysts were characterized with XRD, HRTEM, DRS, PL, XPS, EIS, and photo-responsivity measurements. As compared to catalysts with other compositions, 10% La-doped Zn(O,S) showed better PL spectra, lower electron transfer resistance, and higher photo current, therefore it was used for 4-NP reduction. The photocatalytic detoxification of yellowish 4-NP solution to colorless 4-AP solution was initially identified with the absorbance peak shift from 316.4 nm to 298.7 nm in UV–vis spectra. Furthermore, to ensure the 4-NP conversion to 4-AP, HPLC analysis was done and it showed a complete detoxification of 30 ppm 4-NP could be achieved with 2-hour photo reaction. The photo detoxification of 4-NP was related to the availability of H^+ ions which were produced during the photocatalytic reaction on catalyst surfaces in 10% ethanol solution. This work had shown a promising chemical synthesis route, not only to convert 4-NP to 4-AP but also to possibly catalyze other hydrogenation reactions by utilizing the hydrogen evolution photocatalyst.

Acknowledgment

This work was supported by the Ministry of Science and Technology of Taiwan under Grant number MOST 106-2633-E-011-002 and MOST 107-2221-E-011-141-MY3.

Appendix A. Supplementary data

Supplementary material related to this article can be found, in the online version, at doi: https://doi.org/10.1016/j.jhazmat.2018.09.030.

References

[1] Toxicological profile for 4-nitrophenol, Agency for Toxic Substances and Disease Registry, U.S. Public Health Service, July 1992.
[2] O. Ahmed Zelekew, D.-H. Kuo, A two-oxide nanodiode system made of double-layered p-type Ag_2O@n-type TiO_2 for rapid reduction of 4-nitrophenol, J. Chem. Soc. Faraday Trans. 18 (2016) 4405–4414.
[3] M.M. Mohamed, M.S. Al-Sharif, Visible light assisted reduction of 4-nitrophenol to 4-aminophenol on Ag/TiO_2 photocatalysts synthesized by hybrid templates, Appl. Catal. B 142–143 (2013) 432–441.
[4] D. Xu, P. Diao, T. Jin, Q. Wu, X. Liu, X. Guo, H. Gong, F. Li, M. Xiang, Y. Ronghai, Iridium oxide nanoparticles and Iridium/Iridium oxide nanocomposites: photochemical fabrication and application in catalytic reduction of 4-Nitrophenol, ACS Appl. Mater. Interfaces 7 (2015) 16738–16749.
[5] Y.-C. Chang, D.-H. Chen, Catalytic reduction of 4-nitrophenol by magnetically recoverable Au nanocatalyst, J. Hazard. Mater. 165 (2009) 664–669.
[6] A.L. Luna, D. Dragoe, K. Wang, P. Beaunier, E.K. Kowalska, B. Ohtani, D. Bahena Uribe, M.A. Valenzuela, H. Remita, C. Colbeau-Justin, Photocatalytic hydrogen evolution using Ni-Pd/TiO_2: correlation of light absorption, charge-carrier dynamics and quantum efficiency, J. Phys. Chem. C (2017).
[7] L. Lunar, D. Sicilia, S. Rubio, D. Pérez-Bendito, U. Nickel, Degradation of photographic developers by Fenton's reagent: condition optimization and kinetics for metol oxidation, Water Res. 34 (2000) 1791–1802.
[8] H. Abdullah, D.-H. Kuo, Facile synthesis of n-type $(AgIn)_xZn_{2(1-x)}S_2$/p-type Ag_2S nanocomposite for visible light photocatalytic reduction to detoxify hexavalent chromium, ACS Appl. Mater. Interfaces 7 (2015) 26941–26951.
[9] https://en.wikipedia.org/wiki/Median_lethal_dosehttps://www.spectrumchemical.com/MSDS/A6051.pdfhttps://www.atsdr.cdc.gov/toxprofiles/tp50.pdf (Accessed 1st August 2018).
[10] H. Abdullah, N.S. Gultom, D.-H. Kuo, A simple one-pot synthesis of Zn(O,S)/Ga_2O_3 nanocomposite photocatalyst for hydrogen production and 4-nitrophenol reduction, New J. Chem. 41 (2017) 12397–12406.
[11] H. Abdullah, D.-H. Kuo, X. Chen, High efficient noble metal free Zn(O,S) nanoparticles for hydrogen evolution, Int. J. Hydrogen Energy 42 (2017) 5638–5648.
[12] H.-L. Cao, H.-B. Huang, Z. Chen, B. Karadeniz, J. Lü, R. Cao, Ultrafine silver nanoparticles supported on a conjugated microporous polymer as high-performance nanocatalysts for nitrophenol reduction, ACS Appl. Mater. Interfaces 9 (2017) 5231–5236.
[13] Z.D. Pozun, S.E. Rodenbusch, E. Keller, K. Tran, W. Tang, K.J. Stevenson, G. Henkelman, A systematic investigation of p-Nitrophenol reduction by bimetallic dendrimer encapsulated nanoparticles, J. Phys. Chem. C 117 (2013) 7598–7604.
[14] S. RD, Revised effective ionic radii and systematic studies of interatomic distances in halides and chalcogenides, Acta Crystallogr. Sect. A: Cryst. Phys. Diffr. Theor. Gen. Crystallogr. 32 (1976).
[15] H. Abdullah, D.-H. Kuo, Y.-H. Chen, High-efficient n-type TiO_2/p-type Cu_2O nanodiode photocatalyst to detoxify hexavalent chromium under visible light irradiation, J. Mater. Sci. 51 (2016) 8209–8223.
[16] T.R.N. Kutty, A controlled copper-coating method for the preparation of ZnS: Mn DC electroluminescent powder phosphors, Mater. Res. Bull. 26 (1991) 399–406.
[17] J.F. Moulder, J. Chastain, R.C. King, Handbook of X-ray Photoelectron Spectroscopy: a Reference Book of Standard Spectra for Identification and Interpretation of XPS Data, Physical Electronics, Eden Prairie, MN, 1995.
[18] X.Y. Chen, D.H. Kuo, D.F. Lu, N-doped mesoporous TiO_2 nanoparticles synthesized by using biological renewable nanocrystalline cellulose as template for the degradation of pollutants under visible and sun light, Chem. Eng. J. 295 (2016) 192–200.
[19] M. Li, G. Chen, Revisiting catalytic model reaction p-nitrophenol/$NaBH_4$ using metallic nanoparticles coated on polymeric spheres, Nanoscale 5 (2013) 11919–11927.
[20] T. Aditya, J. Jana, N.K. Singh, A. Pal, T. Pal, Remarkable Facet Selective Reduction of 4-Nitrophenol by Morphologically Tailored (111) Faceted Cu2O Nanocatalyst, ACS Omega 2 (2017) 1968–1984.

ORIGINALITY REPORT

25%	10%	24%	10%
SIMILARITY INDEX	INTERNET SOURCES	PUBLICATIONS	STUDENT PAPERS

PRIMARY SOURCES

1	Yong-Xuan Hou, Hairus Abdullah, Dong-Hau Kuo, Sy-Jye Leu, Noto Susanto Gultom, Chi-Hung Su. "A comparison study of SiO 2 /nano metal oxide composite sphere for antibacterial application", Composites Part B: Engineering, 2017 Publication	2%
2	Hairus Abdullah, Noto Susanto Gultom, Dong-Hau Kuo, Albert Daniel Saragih. " Hydrazine-modified Zn-oxysulfide nanoparticles for CO reduction under low UV-light illumination ", Journal of Physics: Conference Series, 2019 Publication	2%
3	Fekadu Tadesse Bekena, Hairus Abdullah, Dong-Hau Kuo, Misganaw Alemu Zeleke. "Photocatalytic reduction of 4-nitrophenol using effective hole scavenger over novel Mg-doped Zn(O,S) nanoparticles", Journal of Industrial and Engineering Chemistry, 2019 Publication	2%
	Submitted to University College London	

4	Student Paper	1%
5	Hairus Abdullah, Dong-Hau Kuo. " Facile Synthesis of n-type (AgIn) Zn S /p-type Ag S Nanocomposite for Visible Light Photocatalytic Reduction To Detoxify Hexavalent Chromium ", ACS Applied Materials & Interfaces, 2015 Publication	1%
6	Hairus Abdullah, Noto Susanto Gultom, Dong-Hau Kuo. "Indium oxysulfide nanosheet photocatalyst for the hexavalent chromium detoxification and hydrogen evolution reaction", Journal of Materials Science, 2017 Publication	1%
7	Lalisa Wakjira Duresa, Dong-Hau Kuo, Kedir Ebrahim Ahmed, Misganaw Alemu Zeleke, Hairus Abdullah. " Highly enhanced photocatalytic Cr( ) reduction using In-doped Zn(O,S) nanoparticles ", New Journal of Chemistry, 2019 Publication	1%
8	Noto Susanto Gultom, Hairus Abdullah, Dong-Hau Kuo, Wen-Cheng Ke. " Oriented p–n Heterojunction Ag O/Zn(O,S) Nanodiodes on Mesoporous SiO for Photocatalytic Hydrogen Production ", ACS Applied Energy Materials, 2019	1%

Publication

9	Ting Li, Shanyu Quan, Xuefeng Shi, Cong Liu, Linmei Yang. " Photocatalytic Activity of Bi O Enhanced by the Addition of Ce /Ce Synthesized by Ethylene Glycol-assisted Solvothermal Method ", ChemistrySelect, 2020 Publication	1%
10	www.mdpi.com Internet Source	1%
11	Kuan-Ting Chuang, Hairus Abdullah, Sy-Jye Leu, Kou-Bin Cheng, Dong-Hau Kuo, Hsin-Chieh Chen, Jian-Hao Chien, Wan-Ting Hu. "Metal oxide composite thin films made by magnetron sputtering for bactericidal application", Journal of Photochemistry and Photobiology A: Chemistry, 2017 Publication	1%
12	Noto Susanto Gultom, Hairus Abdullah, Dong-Hau Kuo. "Facile synthesis of cobalt-doped (Zn,Ni)(O,S) as an efficient photocatalyst for hydrogen production", Journal of the Energy Institute, 2019 Publication	1%
13	Hairus Abdullah, Noto Susanto Gultom, Dong-Hau Kuo, Albert Daniel Saragih. "Effect of Zn(O,S) Synthesis Temperature to Photocatalytic Hydrogen Evolution	1%

Performance", Journal of Physics: Conference Series, 2019
Publication

14	Venkatesan Jayaraman, Alagiri Mani. "Optical, photocatalytic properties of novel pyro- stannate A2Sn2O7 (A=Ce, Ca, Sr), and Pt deposited (SrCe)2Sn2O7 for the removal of organic pollutants under direct solar light irradiation", Materials Science in Semiconductor Processing, 2019 Publication	1%
15	Submitted to University of Leeds Student Paper	1%
16	Noto Susanto Gultom, Hairus Abdullah, Dong-Hau Kuo, Pintor Simamora, Makmur Sirait. "Development photocatalyst reduce graphene oxide (RGO) composited with (Zn,Ni)(O,S) for photocatalytic hydrogen production", Journal of Physics: Conference Series, 2019 Publication	<1%
17	www.nature.com Internet Source	<1%
18	china.iopscience.iop.org Internet Source	<1%
19	eprints.soton.ac.uk Internet Source	<1%

20	Fekadu Tadesse Bekena, Dong-Hau Kuo, Worku Lakew Kebede. "Universal and highly efficient degradation performance of novel Bi2(O,S)3/Mo(O,S)2 nanocomposite photocatalyst under visible light", Separation and Purification Technology, 2020 Publication	<1%
21	philpapers.org Internet Source	<1%
22	Huihui Wang, Ning Zhang, Gong Cheng, Han Guo, Zewen Shen, Lu Yang, Yushan Zhao, Ahmed Alsaedi, Tasawar Hayat, Xiangke Wang. "Preparing a photocatalytic Fe doped TiO2/rGO for enhanced bisphenol A and its analogues degradation in water sample", Applied Surface Science, 2020 Publication	<1%
23	A LIMA. "Evaluation of Geochemical Background at Regional and Local Scales by Fractal Filtering TechniqueCase Studies in Selected Italian Areas", Environmental Geochemistry, 2008 Publication	<1%
24	Noto Susanto Gultom, Hairus Abdullah, Dong-Hau Kuo. "Phase transformation of bimetal zinc nickel oxide to oxysulfide photocatalyst with its exceptional performance to evolve hydrogen",	<1%

Applied Catalysis B: Environmental, 2020
Publication

25 S. Jafar Hoseini, Mehrangiz Bahrami, Nazanin Sadri, Nahal Aramesh et al. "Multi-metal nanomaterials obtained from oil/water interface as effective catalysts in reduction of 4-nitrophenol", Journal of Colloid and Interface Science, 2018 <1%
Publication

26 Seung Wook Shin, M.P. Suryawanshi, Hee Kyeung Hong, Gun Yun, DongHa Lim, Jaeyeong Heo, Soon Hyung Kang, Jin Hyeok Kim. "Strategy for enhancing the solar-driven water splitting performance of TiO 2 nanorod arrays with thin Zn(O,S) passivated layer by atomic layer deposition", Electrochimica Acta, 2016 <1%
Publication

27 Jian Rong, Fengxian Qiu, Tao Zhang, Yao Zhu, Jicheng Xu, Qing Guo, Xiaoming Peng. "Non-noble metal@carbon nanosheet derived from exfoliated MOF crystal as highly reactive and stable heterogeneous catalyst", Applied Surface Science, 2018 <1%
Publication

28 Submitted to University of Keele <1%
Student Paper

29	Margi Jani, Dhyey Raval, Ranjan Kumar Pati, Indrajit Mukhopadhyay, Abhijit Ray. "Effect of annealing atmosphere on microstructure, optical and electronic properties of spray-pyrolysed In-doped Zn(O,S) thin films", Bulletin of Materials Science, 2018 Publication	<1%
30	Submitted to Universitas Prima Indonesia Student Paper	<1%
31	Xiaoyun Chen, Dong-Hau Kuo, Zong-Yan Wu, Hairus Abdullah, Jubin Zhang, Jinguo Lin. "Bimetal Seleno-Sulfide CuNiSeS Nanosheet Catalyst for Methylene Blue Degradation under Dark", European Journal of Inorganic Chemistry, 2018 Publication	<1%
32	sintadev.ristekdikti.go.id Internet Source	<1%
33	eprints.utas.edu.au Internet Source	<1%
34	Angaw Kelemework Abay, Dong-Hau Kuo, Xiaoyun Chen, Albert Daniel Saragih. "A new V-doped Bi 2 (O,S) 3 oxysulfide catalyst for highly efficient catalytic reduction of 2-nitroaniline and organic dyes", Chemosphere, 2017 Publication	<1%

35	d-scholarship.pitt.edu Internet Source	<1%
36	Osman Ahmed Zelekew, Dong-Hau Kuo, Hairus Abdullah. "Synthesis of (Sn,Zn)(O,S) bimetallic oxysulfide catalyst for the detoxification of Cr+6 in aqueous solution", Advanced Powder Technology, 2019 Publication	<1%
37	www.conference.bonfring.org Internet Source	<1%
38	Hsu, Kai-Chih, and Dong-Hwang Chen. "Green synthesis and synergistic catalytic effect ofAg/reduced graphene oxide nanocomposite", Nanoscale Research Letters, 2014. Publication	<1%
39	Atul Verma, Sanath Kumar, Wen-Ku Chang, Yen-Pei Fu. " Bi-functional Ag-Cu O/g-C N hybrid catalysts for the reduction of 4-nitrophenol and the electrochemical detection of dopamine ", Dalton Transactions, 2020 Publication	<1%
40	www.beilstein-journals.org Internet Source	<1%
41	Ying Zhang, Jiabin Zhou, Zhen Li, Qinqin Feng. "Photodegradation pathway of rhodamine B with novel Au nanorods @ ZnO microspheres driven	<1%

by visible light irradiation", Journal of Materials Science, 2017
Publication

42	Submitted to Sungkyunkwan University Student Paper	<1%
43	Yang, Ying, Xinsong Li, Feng Yang, Wen Zhang, Xin Zhang, and Yang Ren. "New route toward integrating large nickel nanocrystals onto mesoporous carbons", Applied Catalysis B Environmental, 2015. Publication	<1%
44	Yang, Jinglei, Xiaoping Shen, Guoxing Zhu, Zhenyuan Ji, and Hu Zhou. "ZnNi alloy nanoparticles grown on reduced graphene oxide nanosheets and their magnetic and catalytic properties", RSC Advances, 2014. Publication	<1%
45	Nakajima, H.. "Electrodeposition of metallic molybdenum films in ZnCl"2-NaCl-KCl-MoCl"3 systems at 250^oC", Electrochimica Acta, 20060505 Publication	<1%
46	Fu Yang, Bangbang Wang, Hang Su, Shijian Zhou, Yan Kong. "Facilely self-reduced generation of Ag nanowires in the confined reductive siliceous nanopores and its catalytic reduction property", Journal of Alloys and	<1%

Compounds, 2017
Publication

47	iopscience.iop.org Internet Source	<1%
48	Morales, M.V., M. Rocha, C. Freire, E. Asedegbega-Nieto, E. Gallegos-Suarez, I. Rodríguez-Ramos, and A. Guerrero-Ruiz. "Development of highly efficient Cu versus Pd catalysts supported on graphitic carbon materials for the reduction of 4-nitrophenol to 4-aminophenol at room temperature", Carbon, 2017. Publication	<1%
49	Hairus Abdullah, Dong-Hau Kuo, Yen-Hung Chen. "High-efficient n-type TiO2/p-type Cu2O nanodiode photocatalyst to detoxify hexavalent chromium under visible light irradiation", Journal of Materials Science, 2016 Publication	<1%
50	Mohamad M. Ayad, Wael A. Amer, Mohammed G. Kotp. "Magnetic polyaniline-chitosan nanocomposite decorated with palladium nanoparticles for enhanced catalytic reduction of 4-nitrophenol", Molecular Catalysis, 2017 Publication	<1%
51	Zhenxing Li, Miao He, Yangyang Wen, Xin Zhang et al. "Highly Monodisperse Cu–Sn Alloy	<1%

Nanoplates for Efficient Nitrophenol Reduction Reaction via Promotion Effect of Tin", Inorganic Chemistry, 2020
Publication

---

52 Wen-chao Peng, Ying Chen, Xiao-yan Li. "MoS2/reduced graphene oxide hybrid with CdS nanoparticles as a visible light-driven photocatalyst for the reduction of 4-nitrophenol", Journal of Hazardous Materials, 2016 <1%
Publication

---

53 worldwidescience.org <1%
Internet Source

---

54 Submitted to University of Nottingham <1%
Student Paper

---

55 Sarvesh Kumar Srivastava, Maria Guix, Oliver G. Schmidt. "Wastewater Mediated Activation of Micromotors for Efficient Water Cleaning", Nano Letters, 2015 <1%
Publication

---

56 Venkatesan Jayaraman, Chinnadurai Ayappan, Baskaran Palanivel, Alagiri Mani. " Bridging and synergistic effect of the pyrochlore like Bi Zr O structure with robust CdCuS solid solution for durable photocatalytic removal of the organic pollutants ", RSC Advances, 2020 <1%
Publication

Guoqing Wu, Xiaoyu Liang, Lijuan Zhang,

57 Zhiyong Tang, Mohammad Al-Mamun, Huijun Zhao, Xintai Su. "Fabrication of Highly Stable Metal Oxide Hollow Nanospheres and Their Catalytic Activity toward 4-Nitrophenol Reduction", ACS Applied Materials & Interfaces, 2017 <1%
Publication

58 Hairus Abdullah, Dong-Hau Kuo, Jiunn-Yih Lee, Chang-Mou Wu. "Recyclability of thin nylon film-supported p-CuBiS2/n-TiO2 heterojunction-based nanocomposites for visible light photocatalytic degradation of organic dye", Applied Physics A, 2016 <1%
Publication

59 Di Xu, Peng Diao, Tao Jin, Qingyong Wu, Xiaofang Liu, Xin Guo, Hongyu Gong, Fan Li, Min Xiang, Yu Ronghai. "Iridium Oxide Nanoparticles and Iridium/Iridium Oxide Nanocomposites: Photochemical Fabrication and Application in Catalytic Reduction of 4-Nitrophenol", ACS Applied Materials & Interfaces, 2015 <1%
Publication

60 Venkatesan Jayaraman, Baskaran Palanivel, Chinnadurai Ayappan, Muthamizhchelvan Chellamuthu, Alagiri Mani. "CdZnS solid solution supported Ce2Sn2O7 pyrochlore photocatalyst that proves to be an efficient candidate towards <1%

the removal of organic pollutants", Separation and Purification Technology, 2019

Publication

Exclude quotes	Off	Exclude matches	Off
Exclude bibliography	On		